Spin-polarized electron transfer in ferromagnet/C$_{60}$ interfaces

Timothy Moorsom,[1] May Wheeler,[1] Taukeer Mohd Khan,[1] Fatma Al Ma'Mari,[1] Christian Kinane,[2] Sean Langridge,[2]
David Ciudad,[3] Amílcar Bedoya-Pinto,[3] Luis Hueso,[3] Gilberto Teobaldi,[4] Vlado K. Lazarov,[5] Daniel Gilks,[5] Gavin Burnell,[1]
Bryan J. Hickey,[1] and Oscar Cespedes[1,*]

[1]*School of Physics and Astronomy, EC Stoner Building, University of Leeds, Leeds LS2 9JT, United Kingdom*
[2]*ISIS, Science and Technology Facilities Council, Rutherford Appleton Laboratory, Harwell Oxford, Didcot OX11 0QX, United Kingdom*
[3]*CIC NanoGUNE, Tolosa Hiribidea, 76, E-20018 Donostia–San Sebastian, Spain*
[4]*University of Liverpool, Department of Chemistry, Crown Street, Liverpool L69 7ZD, United Kingdom*
[5]*Department of Physics, University of York, Heslington, York YO10 5DD, United Kingdom*
(Received 29 April 2014; revised manuscript received 18 August 2014; published 22 September 2014)

The contact between a molecule and a metallic electrode contributes to or even determines the characteristics of organic devices, such as their electronic properties. This is partly due to the charge transfer that takes place when two materials with different chemical potentials are put together. In the case of magnetic electrodes, the transfer can be accompanied by the transmission of a net spin polarization or *spin doping*. In nanocarbon systems, hybridization and spin doping can suppress the moment of a transition metal ferromagnet through the loss of majority spin electrons to the organic. Here, C$_{60}$ is shown to become ferromagnetic as a result of spin doping from cobalt with an induced moment of 1.2 μ_B per cage while suppressing the moment of the ferromagnet by up to 21%. Polarized neutron reflectivity and x-ray magnetic circular dichroism reveal the presence of an antiferromagnetic coupling of the interfacial layers of cobalt and C$_{60}$, and weakly coupled induced magnetism propagating into the bulk organic. Thus, it is shown that the deposition of molecules with high electron affinity can be used to induce zero-voltage spin injection.

PACS number(s): 81.07.Pr, 75.70.Cn

I. INTRODUCTION

Buckminsterfullerene, C$_{60}$, is an excellent candidate for charge transfer applications due to its exhibition of a number of desirable properties, such as low spin orbit coupling, thermal and mechanical resilience, and a mobility of 11 cm^2 /V s, which has permitted its use in organic field effect transistors (OFETs) [1,2]. Though C$_{60}$ is usually diamagnetic, it has demonstrated a number of interesting magnetic properties useful for organic spintronics such as the generation of transient triplet states and an exceptionally large spin diffusion length of 110 nm at room temperature [3,4] and a magnetically ordered state at low T formed in tetrakis(dimethylamino)ethylene (TDAE)-[C$_{60}$] compounds [5,6]. As such, there has been a concerted effort to build spintronic devices, such as spin valves, utilizing C$_{60}$ [7,8]. The molecule has now successfully been incorporated into magnetic field-dependent field effect transistors and spin-dependent, single molecule transport has been measured [9,10]. It has become clear that the interfaces between organic and inorganic materials are particularly salient in the engineering of the properties of a hybrid material [11]. Most intriguing from a materials perspective is the zero bias charge transfer which occurs when materials with disparate chemical potentials, such as metals and organics, are brought into contact. For ferromagnetic metals, this transfer also manifests a transfer of spin polarization, dubbed spin doping. Though the importance of the interface in hybrid materials is well established, the phenomenon of spin doping has yet to be fully explored. Green's function models of nanotubes on ferromagnetic substrates have predicted a measurable induced moment as a result of charge transfer [12] and magnetic force

microscopy (MFM) studies of carbon nanotubes (CNTs) and magnetometry of graphite from the Canyon Diablo meteorite provide experimental confirmation that the formation of an interface between carbon nanomaterials and ferromagnets can significantly alter the properties of the organic due to the formation of hybridized $3d_z/\pi$ bonded p_z orbitals [13,14]. In C$_{60}$, a spin doping effect is expected at transition metal/organic interfaces due to the molecules' high first electron affinity, 2.6 eV, and Fermi level pinning at the interface [15,16]. However, in addition to such effects on the organic, it has also been noted that charge transfer can significantly alter the properties of the underlying ferromagnet [17]. In order to comprehend the mechanisms of charge transfer and, especially, spin doping, there must be a comprehensive investigation of the properties of organic/ferromagnetic interfaces.

II. EXPERIMENT

A. Growth and characterization

Hybrid fullerene/ferromagnetic devices were deposited through a combination of dc magnetron sputtering and *in situ* thermal sublimation in UHV conditions. Atomic force microscopy (AFM) scans of the resultant structures indicate a roughness of metallic/fullerene bilayers of 0.5–1 nm. Cross sectional transmission electron microscopy (TEM) indicates very little interdiffusion of C$_{60}$ and metal occurs even when multilayers are deposited such that energetic, dc sputtered metal atoms impact the C$_{60}$ surface [Fig. 1(a)].

Cobalt deposited in this manner is crystalline and continuous despite the rough C$_{60}$ surface provided a Ta seed layer is used before the first cobalt layer [Figs. 1(b) and 1(c)]. The roughness of the evaporated C$_{60}$ layers is 1–1.5 nm [Fig. 1(d)]. Bilayer structures were deposited using this method which

*Corresponding author: O.Cespedes@leeds.ac.uk
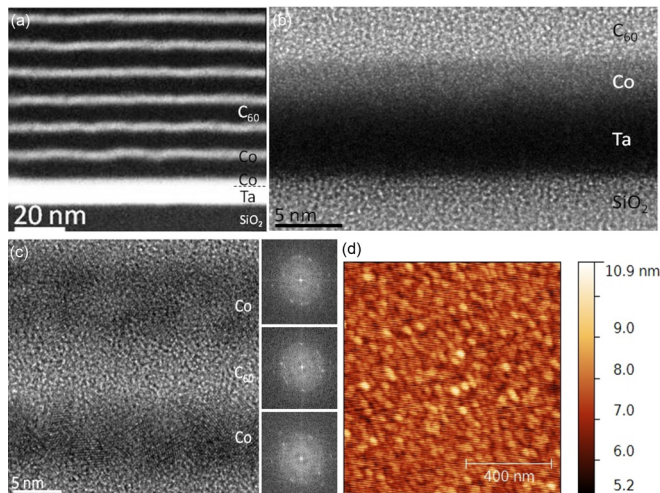
FIG. 1. (Color online) (a) Cross sectional TEM for a multilayer structure of Co/C$_{60}$ with 5 nm of Co and 10 nm of C$_{60}$ using a Ta seed layer. Co layers remain continuous and show little intermixing despite the deposition of metal atoms onto the fullerenes. (b) shows the first layer of Co deposited onto a Ta seed layer and the formation of a crystalline structure. This crystallinity in the Co layers is maintained in subsequent repeats, as demonstrated by the fast Fourier transform (FFT) pattern in (c). The surface roughness for a 50 nm layer of C$_{60}$ is shown in (d) The rms roughness for this film is 1–1.5 nm.

contained 5 nm of Co covered by a layer of C$_{60}$ of varying thickness. Control samples were deposited with a 2 nm Cu film separating the organic from the ferromagnet [see Fig. 2(a), inset]. The presence of this spacer eliminates any hybridization or proximitizing effects across the interface by decoupling the $3d_z$ and π orbitals. The saturation magnetization of Co/C$_{60}$ bilayers with 1–200 nm of C$_{60}$ was shown to be suppressed by 270 $\pm$ 10 emu/cc relative to the control at 100 K [Figs. 2(a) and 2(c)]. Below 100 K, the coercivity of the cobalt loop was shown to increase dramatically [Fig. 2(b)]. This is likely a result of the local pinning sites consisting of uncompensated spins caused by surface defects in the metal and the antiferromagnetic coupling between the first layer of molecules and the ferromagnet. In cobalt/C$_{60}$ interfaces, depression of surface atoms below the C$_{60}$ molecule has also been predicted. These areas of lattice strain could also provide local pinning sites for domain walls [18,19].

The reduction in magnetization can be interpreted as the loss of spin-polarized electrons from the cobalt d band as they are transferred into the organic. A 15% change in the magnetization of a 5 nm cobalt film observed when 20 nm of C$_{60}$ is deposited on top is equivalent to a reduction of $\sim$0.27 μ_B per Co atom. In a simplified analysis, taking an antiferromagnetic coupling between the metal and the organic, the equivalent net transfer is some 0.13 spin-polarized electrons. Given the different atomic densities, the resulting moment is about 2.2 μ_B per C$_{60}$ cage. This would correspond, for example, to a mixture of triplet and quartet states in [C$_{60}$]$^{2-}$ and [C$_{60}$]$^{3-}$.

Van der Waals corrected density functional theory (DFT) simulations and Bader charge analysis [20] for this system reveal that 1.3 electrons are expected to be transferred from the cobalt for each C$_{60}$ placed in contact with the metal

surface, resulting in a change in magnetization of -3.8 μ_B per adsorbed molecule dependent on the orientation of the adsorbed fullerene (Table I).

Electronic structure analysis of the considered C$_{60}$/Co(001) interface model indicates that interfacial hybridization leads to a metallic interface and antiferromagnetic coupling of the carbon atoms closest to the underlying Co(0001), producing a decrease of -1.5 μ_B per cage in the overall interface magnetic moment [Figs. 3(b) and 3(c)]. In spite of the neglect of nonlocal exchange interactions by the adopted functional [Perdew-Burke-Ernzerhof (PBE) [21]], and neglect of further C$_{60}$ layers in the simulations, these results are in agreement with previous PBE-density functional theory (DFT) and experimental results on the magnetic coupling of π-conjugate organics on other (Fe and Cr) magnetic substrates [22,23], which supports the adopted procedure and its conclusions.

B. X-ray magnetic circular dichroism

In order to observe these interfacial effects, x-ray magnetic circular dichroism (XMCD) was used to probe the surface moment of Co/C$_{60}$ bilayers at the MAX-II facility in Lund, Sweden. Two sample constructions were used: one with a continuous, 20 nm thick layer of C$_{60}$ on a 10 nm Co film, and the other with a discontinuous 5 nm C$_{60}$ layer. The samples were measured in a total electron yield (TEY) configuration such that polarization-dependent absorption could be measured by a drain current driven by the emission of free electrons from the sample surface. Both samples were saturated in a field of 150 mT and measured at remanence.

The carbon K edge shows clear asymmetry, particularly in the lowest unoccupied molecular orbital (LUMO) associated peak at 284.5 eV and the π^* antibonding peak [Fig. 4(a)]. This dichroism has a similar magnitude in both the 5 nm and 20 nm C$_{60}$ films (see Fig. S3.3 in the Supplemental Material [24]), indicating a polarization of the LUMO derived band at least 20 nm from the interface [25]. Despite this long range effect, a comparison between the thin and thick C$_{60}$ layers, tantamount to probing the molecules closer to the interface due to the surface sensitivity of the measurement technique [Fig. 4(d)], shows a profound change in the carbon edge approaching the interface [Fig. 4(b)]. Indeed, apart from the suppression of the LUMO, LUMO $+$ 1, and $+$2 peaks. indicating a higher occupation of molecular orbitals, the π^* antibonding peak at 289 eV has the inverse polarization to its counterpart in the thicker sample [26]. In addition, the emergent shoulder at 283.4 eV has the opposite polarization to the L_3 cobalt edge. A similar feature observed by Tran and co-workers in Fe/C$_{60}$ systems was attributed to a partial filling of the LUMO due to interfacial charge transfer [27]. It can be inferred from this shoulder feature that molecules which are at most 5 nm from the interface are involved in hybridization and charge transfer due to their coupling with the ferromagnet. The polarization of this shoulder demonstrates that the induced moment in these fullerenes is antiparallel to the moment of the bulk cobalt. By contrast, the signal in a 20 nm film shows only the LUMO derived peak and no evidence of hybridized interface states. The polarization of the LUMO peak demonstrates that distant molecules will be aligned to the Co film and the applied field. It is possible that the magnetomolecular coupling changes
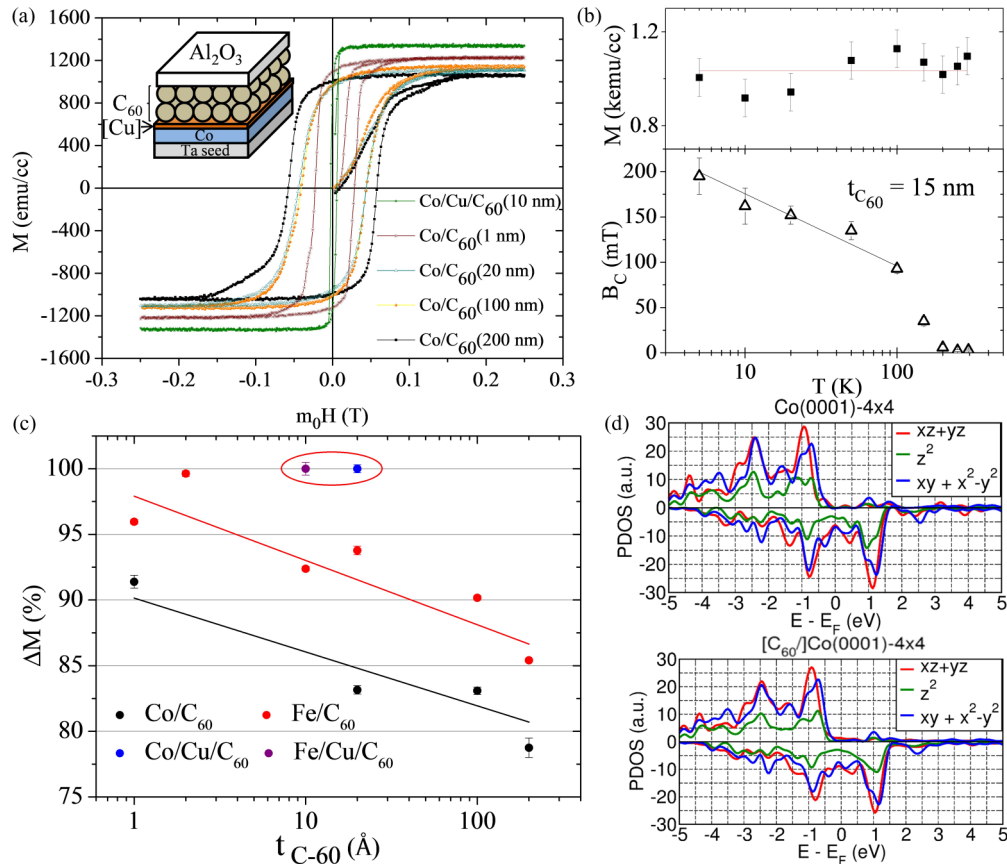
FIG. 2. (Color online) (a) shows the saturation magnetization is suppressed and coercivity enhancement for varying film thicknesses of C_{60} at 100 K. (b) shows the temperature dependence of these changes. The saturation magnetization appears independent of temperature from 10 to 300 K while the coercivity of the loop increases below 100 K. Though even a discontinuous 1 nm layer has a profound effect on the magnetization of the cobalt, the saturation magnetization continues to decrease logarithmically up to 200 nm [(c) black points]. A copper spacer layer [(a) inset] restores the cobalt layer to its pristine condition. DFT models of this system (d) show the distortion of the d band as a result of C_{60}. The changes are most apparent in the polarized density of states (PDOS) for the $3d_z$ band. While hybridization is expected in other transition metals, the effect is considerably reduced in iron [(c) red points] (see Fig. S2.1 in the Supplemental Material [24]), with 200 nm of C_{60} causing a 13% change at 100 K as opposed to 21% in Co. This is due to the stronger $3s$-2π coupling in iron. The effect is entirely absent in nickel.

sign after the first few nm but, given the quick decay of the hybridization and electron transfer away from the interface, it more reasonable to expect that those molecules which are screened by the first monolayer of C_{60} will interact only weakly with the ferromagnet, if at all. As the coupling weakens, the C_{60} would behave paramagnetically, aligning only to the stray field of the Co and/or the applied external field.

TABLE I. Relative energies, adsorption energies, and magnetization changes for a Co(0001) 4 × 4 slab with an adsorbed C_{60} cage in various geometries and with various z separations. The details of these geometries are shown in Fig. 3(a).

Geometry	ΔE (eV)	E_{ads} (eV)	ΔM (μ_B)
h (z_{start}: +3 Å)	+3.77	−1.76	−0.089
h (z_{start}: +2 Å)	+0.20	−5.34	−3.503
hp (z_{start}: +3 Å)	+3.58	−1.95	−0.046
hp (z_{start}: +2 Å)	0.00	−5.53	−3.756
p (z_{start}: +3 Å)	+3.60	−1.94	−0.049
p (z_{start}: +2 Å)	+0.43	−5.10	−3.626

At the cobalt edge, dichroism in the L_2 and L_3 transitions, analyzed using the established sum rules for the transition metal ferromagnets, indicated an M_l/M_s ratio of 0.41 when in contact with a 20 nm C_{60} layer [Fig. 4(c)], to be compared with an expected value of 0.099 in pure cobalt [28]. While the intensity of the cobalt edge would be attenuated by the organic layer, there also exists suppression of the magnetic moment in at least the interfacial region of the cobalt substrate. Distortion of the cobalt d band can be observed as a change in the x-ray photoemission spectrum (XPS), confirming that the presence of C_{60} alters the density of states of the metal (see Fig. S1.6 in the Supplemental Material [24]).

C. Polarized neutron reflectivity

In order to obtain a magnetic profile of the structure, polarized neutron reflectivity (PNR) measurements were performed on cobalt C_{60} superlattices at the ISIS facility in the Rutherford Appleton Laboratory. This technique expands upon the surface sensitive data of XMCD and allows the moment associated with each layer, including the C_{60}, to be calculated [29]. Two samples were observed: a ten layer structure consisting of
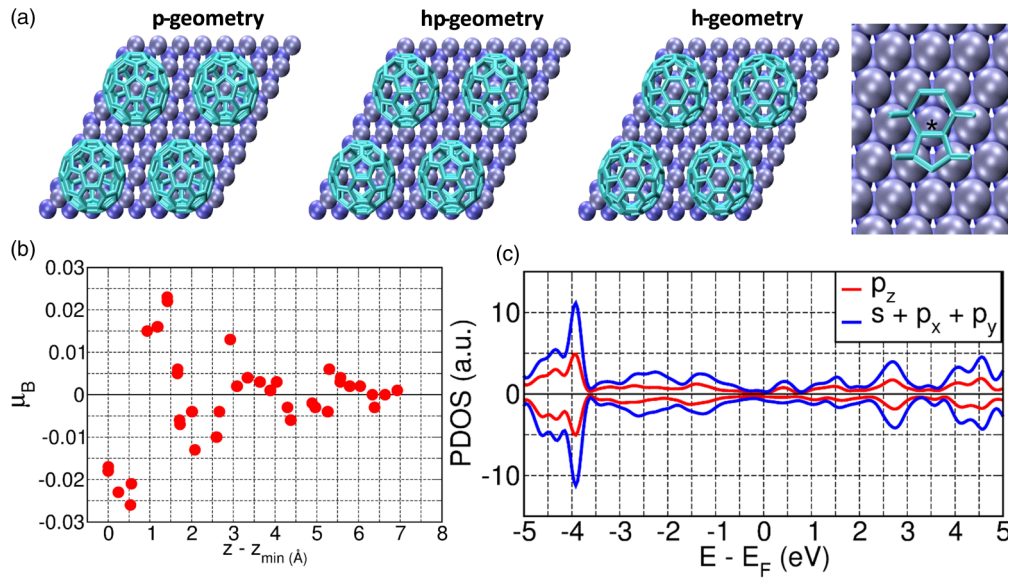
FIG. 3. (Color online) (a) Example of the various geometries used in simulating the Co/C_{60} contact. The indices p, hp, and h refer to which vertex is closest to the cobalt surface, a pentagonal-pentagonal vertex, hexagonal-pentagonal, or hexagonal-hexagonal, respectively. The optimal configuration, hp, is shown in more detail on the right. The atom denoted by an asterisk is displaced by 0.3 Å due to the C_{60} cage. The distribution of the transferred moment in the C_{60} cage is shown in (b). The moment appears to oscillate, beginning antialigned but varying as one moves away from the interface. The highest electron density is expected in the first angstrom of the cage. (c) Shows the PDOS for the adsorbed cage, demonstrating its asymmetrically distorted LUMO derived bands and metallic behavior.
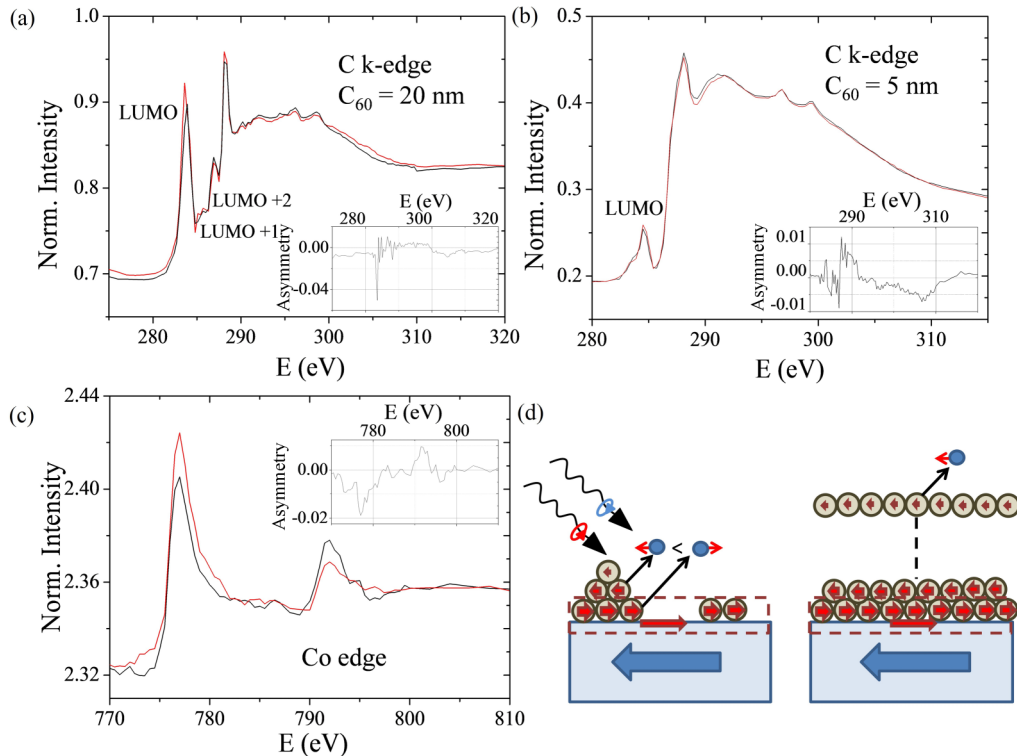
FIG. 4. (Color online) XMCD of a bilayer sample with a 4 nm cobalt film covered with a 20 nm C_{60} film (a) and a discontinuous 5 nm film (b). The insets for both carbon edges track the asymmetry of the absorption spectra for opposite polarizations. The LUMO derived peak is significantly suppressed in the 5 nm sample, indicating a higher occupation. However, the normalized asymmetry of the LUMO peaks is the same for both films. The shoulder feature, however, is only present in the 5 nm film. Cobalt (c) is antiferromagnetically coupled to the hybridized interface state, observable in the shoulder feature of (b), as is clear from the polarization of the L_3 peak and LUMO shoulder. (d) shows the construction of each sample and the resultant different polarization observed in the carbon edge. The expected extent of the interfacial region is highlighted in red.
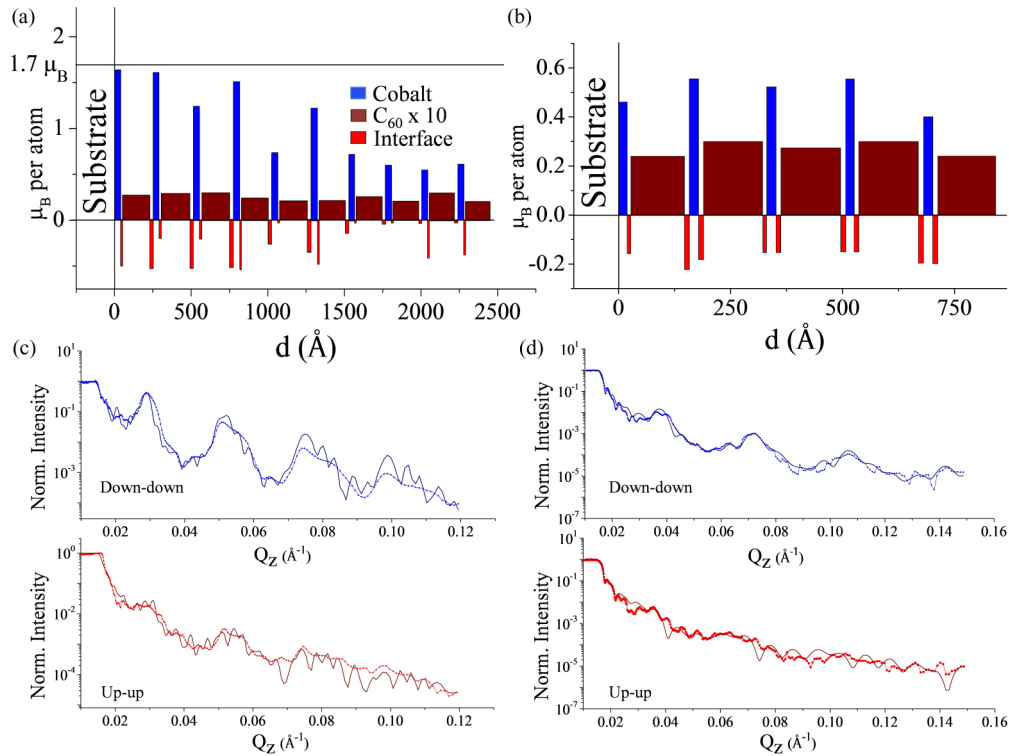
FIG. 5. (Color online) Magnetic profiles for the two multilayer samples: (a) Ta(5 nm)/[Co(4 nm)/C_{60} (21 nm)] $\times$ 10/Al(3 nm) and (b) Ta(5 nm)/[Co(2 nm)/C_{60} (13 nm)] $\times$ 5/Al(3 nm). In both cases, the moment of the C_{60} is multiplied by ten in order to make the differences between layers visible. Reflectivities [(c) and (d)] are fit using GENX software. For higher layer numbers, both interfaces and Co layers become unstable due to the propagation of roughness through the stack.

4 nm cobalt layers and 21 nm C_{60} layers [Fig. 5(a)], and a five layer structure consisting of 2 nm cobalt layers and 13 nm C_{60} layers [Fig. 5(b)]. The samples were saturated in a field of some 300 mT and measured at 150 and 50 mT, respectively, at 300 K by a collimated beam of neutrons from a spallation source. Analysis of the spin-dependent spectra was performed with an optical matrix approach using the GENX PYTHON based, low angle reflectivity fitting program [Figs. 5(c) and 5(d)] [30]. Parameters were constrained by the measured net moment of the sample, the polarization directions extracted from XMCD, and structural information derived from x-ray reflectivity spectra. The interfaces were shown to be consistently antiferromagnetically coupled to the ferromagnet with a moment of up to 0.5 μ_B per atom while the bulk of the organic remains aligned to the ferromagnet. The interfacial region is expected to include at least the first layer of metallic fullerenes and the upper layers of the ferromagnet and is predicted to extend a total of 10 nm, though the upper interface of each C_{60} layer is thicker due to the deposition of metal atoms onto the organic and the resultant small intermixing layer. The average moment of C_{60} in the aligned region is 1.2 μ_B per cage (see Figs. S3.1 and S3.2 in the Supplemental Material [24]).

III. CONCLUSION

The use of multiple magnetic and spin-dependent measurement techniques has formed a detailed picture of the

effect of interfacial hybridization and spin doping in Co/C_{60} hybrid materials. Not only does the transfer of polarized electrons induce a magnetic moment of 0.1 μ_B -3 μ_B per cage in the C_{60}, but the loss of majority spin electrons and changes to the structure of the d band result in a significant loss of magnetization in the ferromagnet. Aside from the spin doping effects observed here, an investigation of the interfacial properties of this system, both computationally and experimentally, reveal the structure of the interface. The antiferromagnetic coupling of at least one layer of metallo-fullerenes to the underlying cobalt, predicted from projector augmented-wave (PAW) sphere calculations and confirmed in XMCD, increase the *BH* product of the film. Such variations in polarization at a metal-organic interface are not unexpected. Indeed, spin transport studies for organic molecules such as Co-phthalocyanine have observed the inversion of interfacial polarization as a result of hybridization [31]. This phenomenon is interpreted in single molecule systems as the result of spin-dependent band broadening and energy level shifting in the organic energy levels [32,33]. PNR and XMCD show that the bulk of the organic experiences only weak coupling to the ferromagnet and remains aligned to the applied field, suggesting a long range diffusion of spin not governed by the same coupling mechanism present at the interface. Even when the molecules are away from the interface, there remains a small charge diffusion into the C_{60} molecules. The reduced anions may still be spin polarized and behave as paramagnets that align only to the external fields and/or the stray field of the ferromagnet. This model of the dependence

of the sign of the molecular moment agrees with both the experimental data and DFT calculations presented herein for the interface, which predict an antiferromagnetic coupling of organic and ferromagnet only for the molecules in contact with the ferromagnet. Remarkably, however, magnetometry reveals that due to the spin-polarized electronic transfer it is not only the interface which affects the metal. Indeed, fullerenes that are 200 nm from the interface still serve to suppress the magnetization of the Co film. An understanding of both the interfacial and long range phenomena observed here will be instrumental in illuminating the mechanisms of charge transfer and spin doping in metallic/organic hybrid systems.

[1] D. M. Gruen, Nucl. Instrum. Methods Phys. Res. **78**, 118 (1993).

[2] H. Li, B. C. K. Tee, J. J. Cha, Y. Cui, J. W. Chung, S. Y. Lee, and Z. N. Bao, J. Am. Chem. Soc. **134**, 2760 (2012).

[3] Z. X. Luo, X. Cheng, Y. Luo, B. H. Loo, A. D. Peng, and J. N. Yao, J. Am. Chem. Soc. **134**, 1130 (2012).

[4] X. M. Zhang *et al.*, Nat. Commun. **4**, 1392 (2013).

[5] A. Lappas, K. Prassides, K. Vavekis, D. Arcon, R. Blinc, P. Cevc, A. Amato, R. Feyerherm, F. N. Gygax, and A. Schenck, Science **267**, 1799 (1995).

[6] F. Wudl and J. D. Thomson, J. Phys. Chem. Solids **53**, 1449 (1992).

[7] T. L. A. Tran, T. Q. Le, J. G. M. Sanderink, W. G. van der Wiel, and M. P. de Jong, Adv. Funct. Mater. **22**, 1180 (2012).

[8] M. Gobbi, F. Golmar, R. Llopis, F. Casanova, and L. E. Hueso, Adv. Mater. **23**, 1609 (2011).

[9] M. Gobbi, A. Bedoya-Pinto, F. Golmar, R. Llopis, F. Casanova, and L. E. Hueso, Appl. Phys. Lett. **101**, 102404 (2012).

[10] A. N. Pasupathy, R. C. Bialczak, J. Martinek, J. E. Grose, L. A. K. Donev, P. L. McEuen, and D. C. Ralph, Science **306**, 86 (2004).

[11] C. Barraud, P. Seneor, R. Mattana, S. Fusil, K. Bouzehouane, C. Deranlot, P. Graziosi, L. Hueso, I. Bergenti, V. Dediu, F. Petroff, and A. Fert, Nat. Phys. **6**, 615 (2010).

[12] M. S. Ferreira and S. Sanvito, Phys. Rev. B **69**, 035407 (2004).

[13] O. Cespedes, M. S. Ferreira, S. Sanvito, M. Kociak, and J. M. D. Coey, J. Phys.: Condens. Matter **16**, L155 (2004).

[14] J. M. D. Coey, M. Venkatesan, C. B. Fitzgerald, A. P. Douvalis, and I. S. Sanders, Nature (London) **420**, 156 (2002).

[15] H. Zettergren, M. Alcami, and F. Martin, Phys. Rev. A **76**, 043205 (2007).

[16] T. R. Ohno, Y. Chen, S. E. Harvey, G. H. Kroll, and J. H. Weaver, Phys. Rev. B **44**, 13747 (1991).

[17] P. K. J. Wong, W. Zhang, K. Wang, G. van der Laan, Y. B. Xu, W. G. van der Wiel, and M. P. de Jong, J. Mater. Chem. C **1**, 1197 (2013).

[18] Y.-J. Hsu, Y.-L. Lai, C.-H. Chen, Y.-C. Lin, H.-Y. Chien, J.-H. Wang, T.-N. Lam, Y.-L. Chan, D. H. Wei, H.-J. Lin, and C.-T. Chen, J. Phys. Chem. Lett. **4**, 310 (2012).

[19] D. Givord, M. F. Rossignol, and D. W. Taylor, J. Phys. IV (France) **2**, C3-95 (1992).

[20] G. Henkelman, A. Arnaldsson, and H. Jonsson, Comput. Mater. Sci. **36**, 354 (2006).

[21] J. P. Perdew, K. Burke, and M. Ernzerhof, Phys. Rev. Lett. **77**, 3865 (1996).

[22] S. L. Kawahara, J. Lagoute, V. Repain, C. Chacon, Y. Girard, S. Rousset, A. Smogunov, and C. Barreteau, Nano Lett. **12**, 4558 (2012).

[23] N. Atodiresei, J. Brede, P. Lazic, V. Caciuc, G. Hoffmann, R. Wiesendanger, and S. Blugel, Phys. Rev. Lett. **105**, 066601 (2010).

[24] See Supplemental Material at http://link.aps.org/supplemental/10.1103/PhysRevB.90.125311 for additional TEM and XPS characterization, details of PNR fitting, additional XMCD discussion, details of DFT calculations and magnetometry of Fe/C_{60} complexes.

[25] P. Y. Cheng, M. R. Chiang, Y. L. Chan, Y. J. Hsu, P. C. Wang, and D. H. Wei, Appl. Phys. Lett. **104**, 043303 (2014).

[26] Y. Saito, H. Shinohara, and A. Ohshita, Jpn. J. Appl. Phys. **30**, L1145 (1991).

[27] T. L. A. Tran, P. K. J. Wong, M. P. de Jong, W. G. van der Wiel, Y. Q. Zhan, and M. Fahlman, Appl. Phys. Lett. **98**, 222505 (2011).

[28] C. T. Chen, Y. U. Idzerda, H. J. Lin, N. V. Smith, G. Meigs, E. Chaban, G. H. Ho, E. Pelledrin, and F. Sette, Phys. Rev. Lett. **75**, 152 (1995).

[29] S. J. Blundell and J. A. C. Bland, Phys. Rev. B **46**, 3391 (1992).

[30] M. Bjorck and G. Andersson, J. Appl. Crystallogr. **40**, 1174 (2007).

[31] J. Brede, N. Atodiresei, S. Kuck, P. Lazic, V. Caciuc, Y. Morikawa, G. Hoffmann, S. Blugel, and R. Wiesendanger, Phys. Rev. Lett. **105**, 047204 (2010).

[32] A. R. Rocha and S. Sanvito, J. Appl. Phys. **101**, 09B102 (2007).

[33] S. Sanvito, Nat. Phys. **6**, 562 (2010).